Ailanthone induces autophagy and ferroptosis in non-small cell lung cancer Lewis cells

HONGBIN YANG[1*], XIAOTONG ZHANG[1*], YANJIE LU[2], XIN WANG[3], ZHENGXIN ZHANG[2], HAILAN XU[3], FAN LI[1], QIANHUI CHEN[3], YIYING BAI[3], XINYU BAI[3], LI ZHANG[3] and LEI LIU[1]

Departments of [1]Immunology and [2]Pathology Chengde Medical University; [3]Department of Oncology, The Affiliated Hospital of Chengde Medical University, Chengde, Hebei 067000, P.R. China

Received November 6, 2023; Accepted January 17, 2024

DOI: 10.3892/mco.2024.2723

Abstract. Ailanthone (AIL), a monomer derived from ailanthus in Chinese medicine, has been demonstrated to have antitumor effects, albeit the underlying mechanism is unknown. Autophagy and ferroptosis are two modes of cell death that have been championed as potential mechanisms implicated in the antitumor effects of various drugs. The present study demonstrated that AIL effectively suppresses the Lewis cell proliferation in non-small cell lung cancer using MTT and colony formation assays. Autophagy and ferroptosis were verified using western blotting, immunofluorescence and ferroptosis detection. Additionally, the findings revealed that regulating the AMPK/mTOR/p70S6k signaling pathway may be the underlying mechanism for the antitumor effect of AIL. The present study established a theoretical foundation for further research into the utilization of AIL as a novel antitumor approach.

Introduction

Lung cancer is the leading cause of cancer-related mortality worldwide, with an exceedingly poor prognosis (1); of these, non-small cell lung cancer (NSCLC) accounts for ~85% (2). The most common lung cancer therapies include surgery, chemotherapy, radiotherapy, targeted therapy and immunotherapy; nevertheless, these treatments do not significantly improve the long-term survival of patients (3). In this view, substantial research has been devoted to developing safe and effective antitumor drugs, including nanoparticles (4,5) and Chinese herbs. Ailanthone (AIL) is one of the most significant active constituents of ailanthus, a traditional Chinese herbal medicine with anti-inflammatory, anti-allergic, anti-malaria and antitumor properties. Previous studies have identified that AIL suppresses various tumors, including glioma, liver carcinoma and leukemia by augmenting apoptosis, autophagy and cell cycle arrest (6-8). However, the effects and mechanisms by which AIL acts on lung cancer have not been fully elucidated.

Autophagy is a self-eating homeostatic catabolic process for the final degradation of intracellular components in lysosomes regulated by the autophagy-related gene (ATG) (9). Autophagy maintains optimal cellular homeostasis under physiological conditions. However, excessive autophagy can result in autophagic cell death and the activation of autophagy signaling pathways (10). Pharmacological agents such as natural small molecules or Chinese herb extracts have been demonstrated to cause autophagic cell death in several cancer types, including NSCLC (11,12). Ferroptosis is a form of iron-dependent programmed cell death that differs from necrosis, apoptosis and autophagy by lipid peroxidation (LPO) and iron accumulation (13). Guo *et al* (14) revealed that a combination of cisplatin and the ferroptosis inducer erastin exhibited increased antitumor activity. In this view, ferroptosis has emerged as an attractive strategy for cancer treatment, with significant implications for lowering lung cancer recurrence and mortality rates, as well as improving patient prognosis. Evidence indicates that an intricate crosstalk exists between autophagy and ferroptosis (15), that ferroptosis is dependent on autophagy, and that excessive autophagy cell activation can increase ferroptosis by degrading ferritin in fibroblasts and cancer cells (16).

AMP-activated protein kinase (AMPK) is a highly conserved serine/threonine protein kinase that acts as an energy sensor, regulating energy metabolism and the ATP-generating rate (17). Recent research indicated that AMPK is implicated in various programmed cell death mechanisms, including apoptosis, necroptosis, autophagy and ferroptosis, depending on the environmental stimuli (18). Activation of the AMPK/mTOR/p70S6k signaling pathway enhances autophagy, promotes ferritin degradation, increases

Correspondence to: Professor Lei Liu, Department of Immunology, Chengde Medical University, Anyuan Road, Chengde, Hebei 067000, P.R. China
E-mail: homingreceptor@hotmail.com

Professor Li Zhang, Department of Oncology, The Affiliated Hospital of Chengde Medical University, 34 Nanyingzi Street, Chengde, Hebei 067000, P.R. China
E-mail: cd_zhangl@126.com

[*]Contributed equally

Key words: ailanthone, autophagy, ferroptosis, non-small cell lung cancer, Lewis cells

the labile iron pool, and accelerates the accumulation of intracellular reactive oxygen species (ROS), eventually causing ferroptosis (19). These findings demonstrated a potential link between the AMPK/mTOR/p70S6k signaling pathway with autophagy and ferroptosis pathways. The present study investigated the role of AIL in inhibiting cell proliferation, promoting cell autophagy and ferroptosis, and regulating the AMPK/mTOR/p70S6k signaling pathway. The findings provide the theoretical groundwork for the development of a novel drug and the clinical application of AIL.

Materials and methods

Cell culture. Mouse NSCLC Lewis cells were purchased from Guangzhou Geneo Biotechnology (https://www.jennio-bio.com/product/829.html?productCateId=59). Meanwhile, mouse normal lung epithelial TC-1 cells were obtained from Procell Life Science & Technology Co., Ltd. and used as a control. All cells were cultured in complete DMEM containing 10% fetal bovine serum, 100 U/ml penicillin, and 100 μg/ml streptomycin (cat. no. P1400-100ml; Beijing Solarbio Science & Technology Co., Ltd.) at 37˚C in a humidified incubator containing 5% CO_2.

MTT assays. Lewis ($1.5x10^4$/well) and TC-1 cells ($5.0x10^3$/well) were seeded in a 96-well plate, incubated for 24 h, and then treated with a gradient concentration of AIL for 24, 36 and 48 h. AIL was purchased from Chengdu Alfa Biological Technology Co. Ltd. (Chengdu, China). Subsequently, 20 μl of MTT at 5 mg/ml was added to each well and incubated for 4 h. The medium was then replaced with 100 μl DMSO to solubilize the formazan crystals. Absorbance was measured at 490 nm wavelength using a microplate reader (BioTek Instruments Inc.).

Colony formation assay. Lewis cells ($1.0x10^3$ cells) were seeded in each 60 mm culture dish and incubated for 24 h, and then treated with varying concentrations of AIL (0, 2.5, 5 and 10 μM) for 24 h. Cells were washed in PBS and incubated at 37˚C in a complete growth medium for two weeks to form clones. The cells were then fixed with 2 ml methanol and stained using crystal violet solution (0.1%) for 30 min at room temperature. Cell survival ability was evaluated by counting clones on each plate. The number of clones forming >50 cells was calculated by ImageJ v.1.8.0 software (National Institutes of Health).

Western blotting. Lewis cells were cultured to 80% confluence in 60 mm dishes and treated with various concentrations of AIL (0, 2.5, 5 and 10 μM) for 24 h. Cells were lysed in RIPA buffer (Beijing Solarbio Science & Technology Co., Ltd.) containing PMSF (RIPA: PMSF=100:1). Protein concentrations were then quantified using a BCA protein assay kit (cat. no. PC0020-50; Beijing Solarbio Science & Technology Co., Ltd.). A 20-microgram amount of protein was loaded on SDS-PAGE and transferred onto a nitrocellulose membrane. The membrane was blocked with 5% BSA (Beijing Solarbio Science & Technology Co., Ltd.) at 37˚C for 3 h, and then incubated overnight at 4˚C with the following primary antibodies: Rabbit microtubule-associated protein light chain3B monoclonal antibody (LC3B; 1:2,000), rabbit sequestosome1 monoclonal antibody (SQSTM1/P62; 1:10,000), rabbit autophagy-related protein 6 polyclonal antibody (ATG6/beclin1; 1:2,000), rabbit autophagy-related protein 5 monoclonal antibody (ATG5; 1:1,000), rabbit solute carrier family 7 member 11 monoclonal antibody (SLC7A11/xCT; 1:10,000), rabbit glutathione peroxidase 4 monoclonal antibody (GPX4; 1:2,000), rabbit ferritin heavy chain monoclonal antibody (FTH; 1:2,000), rabbit transferrin receptor monoclonal antibody (TFRC; 1:2,000), rabbit phospho-AMPK monoclonal antibody (p-AMPK; 1:500), rabbit AMPK monoclonal antibody (1:500), rabbit phospho-mammalian target of rapamycin monoclonal antibody (p-mTOR; 1:500), rabbit mTOR monoclonal antibody (1:10,000), rabbit phospho-ribosomal protein S6 kinase monoclonal antibody (p-p70S6K; 1:2,000), rabbit ribosomal monoclonal antibody (p70S6K; 1:10,000), rabbit nuclear receptor coactivator 4 monoclonal antibody (NCOA4; 1:2,000), and rabbit β-actin monoclonal antibody (1:10,000). After washing with Tris-buffered saline containing 0.05% Tween 20 (TBST), the membranes were incubated with HRP-coupled secondary antibodies (1:5,000; cat. no. AS014; ABclonal Biotech Co., Ltd.) for 2 h at room temperature and visualized with the enhanced chemiluminescence system (Zhongshi Gene Technology Co., Ltd.; http://www.zsgentech.com/). Blots were scanned and examined using ImageJ v.1.8.0 software (National Institutes of Health).

Immunofluorescence. Lewis cells were seeded into 24-well plates ($5x10^4$ cells per well) and incubated for 24 h. The cells were treated with gradient concentrations of AIL (0, 2.5, 5 and 10 μM) for 24 h, fixed with 4% paraformaldehyde for 30 min at room temperature, and solubilized in 0.1% Triton X-100 for 10 min. The cells were then blocked with 5% BSA for 1 h at room temperature and incubated with primary antibodies [rabbit LC3B monoclonal antibody (1:100) and rabbit P62 monoclonal antibody (1:100)] at 4˚C for 4 h, and fluorescently labeled with anti-rabbit secondary antibodies (1:1,000; cat. no. AS011; ABclonal Biotech Co., Ltd.) for 2 h in the dark. Subsequently, cells were stained with DAPI (5 mg/ml; cat. no. C1005; Beyotime Institute of Biotechnology) at room temperature for 3 min, and examined under a fluorescence microscope (Olympus Corporation).

ROS assay. ROS generation was evaluated using a ROS assay kit (cat. no. S0033S; Beijing Solarbio Science & Technology Co., Ltd.) according to the manufacturer's protocol. Lewis cells were seeded into 6-well plates ($5x10^5$ cells per well) and treated on the next day with gradient concentrations of AIL (0, 2.5, 5 and 10 μM) for 24 h. Subsequently, 10 μM 2,7-dichlorodi-hydrofluorescein diacetate (DCFH-DA) was added into each well and incubated in the dark for 20 min. The cells were washed with serum-free medium 3 times, digested, and transferred to a 96-well plate at the same density. The fluorescence intensity was measured at a 488 nm excitation and 525 nm emission wavelength on a fluorescence microplate reader (BioTek Instruments, Inc.). In addition, fluorescence was also directly observed under a fluorescence microscope (Olympus Corporation).

Determination of ferroptosis-related markers. Intracellular levels of Fe^{2+}, LPO, malondialdehyde (MDA), glutathione (GSH), total superoxide dismutase (T-SOD) and catalase (CAT)

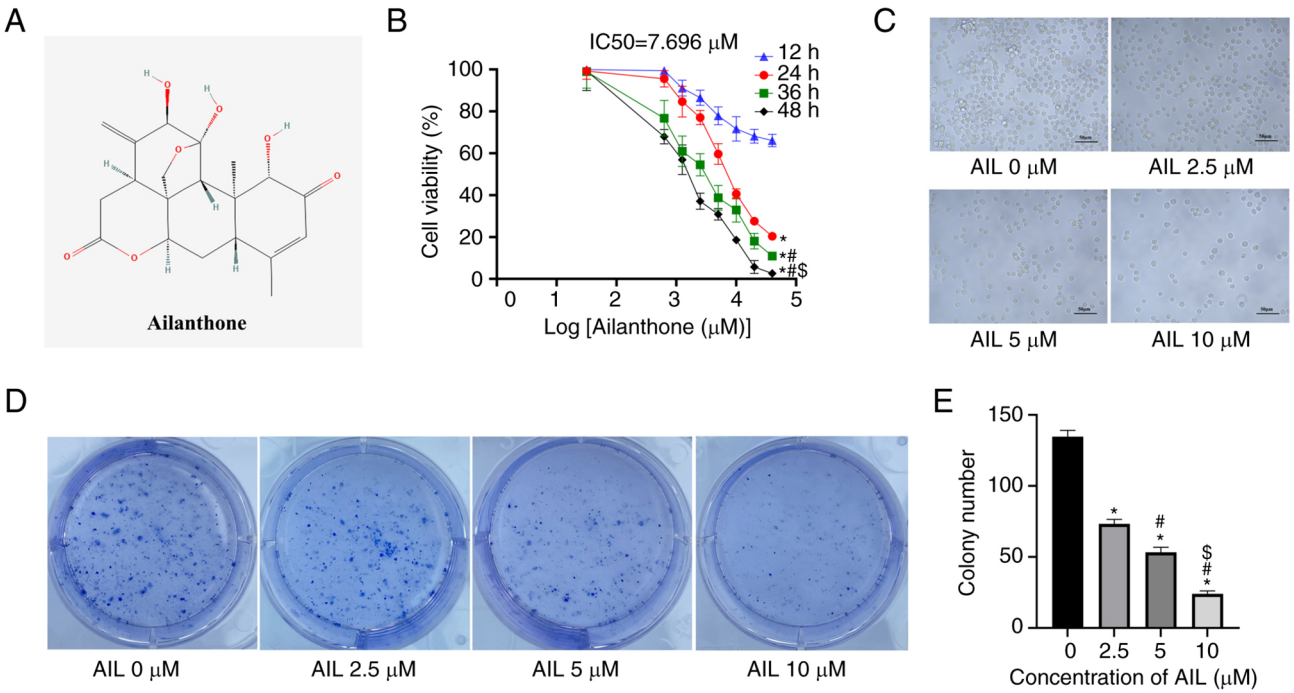

Figure 1. AIL inhibits Lewis cell proliferation. (A) The chemical structure of AIL. (B) MTT assessment of cell viability of Lewis cells after treatment with a gradient concentration of AIL at 12, 24, 36 and 48 h. (C) The Lewis cell morphology after treatment with increasing concentrations of AIL (0, 2.5, 5 and 10 μM). (D) Colony formation assay for the different concentrations of AIL treatment groups. (E) Semi-quantitative analysis of the results from the colony formation assay. *P<0.05 vs. AIL 0 μM group; $^{\#}$P<0.05 vs. AIL 2.5 μM group and $^{\$}$P<0.05 vs. AIL 5 μM group. AIL, ailanthone.

were determined using the Fe^{2+} assay kit (cat. no. A039-2-1), LPO assay kit (cat. no. A106-1-1), MDA assay kit (cat. no. A003-1-1), GSH assay kit (cat. no. A061-1-2), T-SOD assay kit (cat. no. A001-1-1) and CAT assay kit (cat. no. A007-1-1), respectively, following the manufacturer's protocols. All the kits were purchased from Nanjing Jiancheng Bioengineering Institute.

Statistical analysis. All experiments were repeated three times. SPSS 22.0 software (IBM Corp.) was employed for statistical analysis. Data are presented as the mean ± standard deviation. Differences between AIL concentration groups were compared using one-way ANOVA followed by Tukey's post hoc test. P<0.05 was considered to indicate a statistically significant difference.

Results

AIL inhibits the growth of NSCLC Lewis cells. The chemical structure of AIL is depicted in Fig. 1A (PubChem ID, 72965). Lewis and TC-1 cells were treated with a gradient concentration of AIL for different time points (12, 24, 36 and 48 h), and cell viability was assessed by MTT. The findings demonstrated that AIL suppressed Lewis cell viability in a dose- and time-dependent manner (Fig. 1B); the IC_{50} value after 24 h of AIL treatment was 7.696±0.327 μM. Interestingly, AIL did not alter mouse normal lung epithelial cell (TC-1) growth (Fig. S1). Next, Lewis cells were treated with 0, 2.5, 5 or 10 μM AIL for 24 h and their morphology was examined by light microscopy. The cells exhibited poor adhesion and refractivity ability and uneven-size shrunk cells with an increase in AIL concentration (Fig. 1C). Furthermore, the influence of AIL on cell proliferation was evaluated using the cell colony formation test. The results demonstrated that the number of cell colony formations decreased significantly as the AIL dosage increased (F=0.680, P<0.001; Fig. 1D and E). These findings demonstrated that AIL significantly inhibited the growth of NSCLC Lewis cells.

AIL induces autophagy in NSCLC Lewis cells. The potential of AIL to regulate autophagy was assessed based on the expression level of several autophagy-associated proteins in Lewis cells after treatment with 0, 2.5, 5 or 10 μM AIL for 24 h. As illustrated in Fig. 2A and B, the protein expression levels of Beclin1 (F=456.014; P<0.001), ATG5 (F=247.187; P<0.001) and LC3B (F=152.740; P<0.001) increased, while the expression of P62 (F=1234.348; P<0.001) decreased with an increase in AIL concentration. The immunofluorescence results were consistent with the findings of western blot experiments in which an increase in AIL concentration increased the green fluorescence intensity of LC3B (F=152.179; P<0.001; Fig. 2C and D) but decreased the green fluorescence intensity of P62 (F=255.494; P<0.001; Fig. 2E and F).

AIL induces ferroptosis in NSCLC Lewis cells. ROS accumulation is one of the hallmarks of ferroptosis; therefore, ROS levels in Lewis cells treated with a gradient concentration of AIL were assessed using the ROS-detecting fluorescent dye DCFH-DA. The results obtained by fluorescence microscopy (F=182.200; P<0.001; Fig. 3A and B) and a fluorescent microplate reader (F=15.863; P<0.001; Fig. 3C) revealed that the green fluorescence intensity increased with an increase in AIL concentrations.

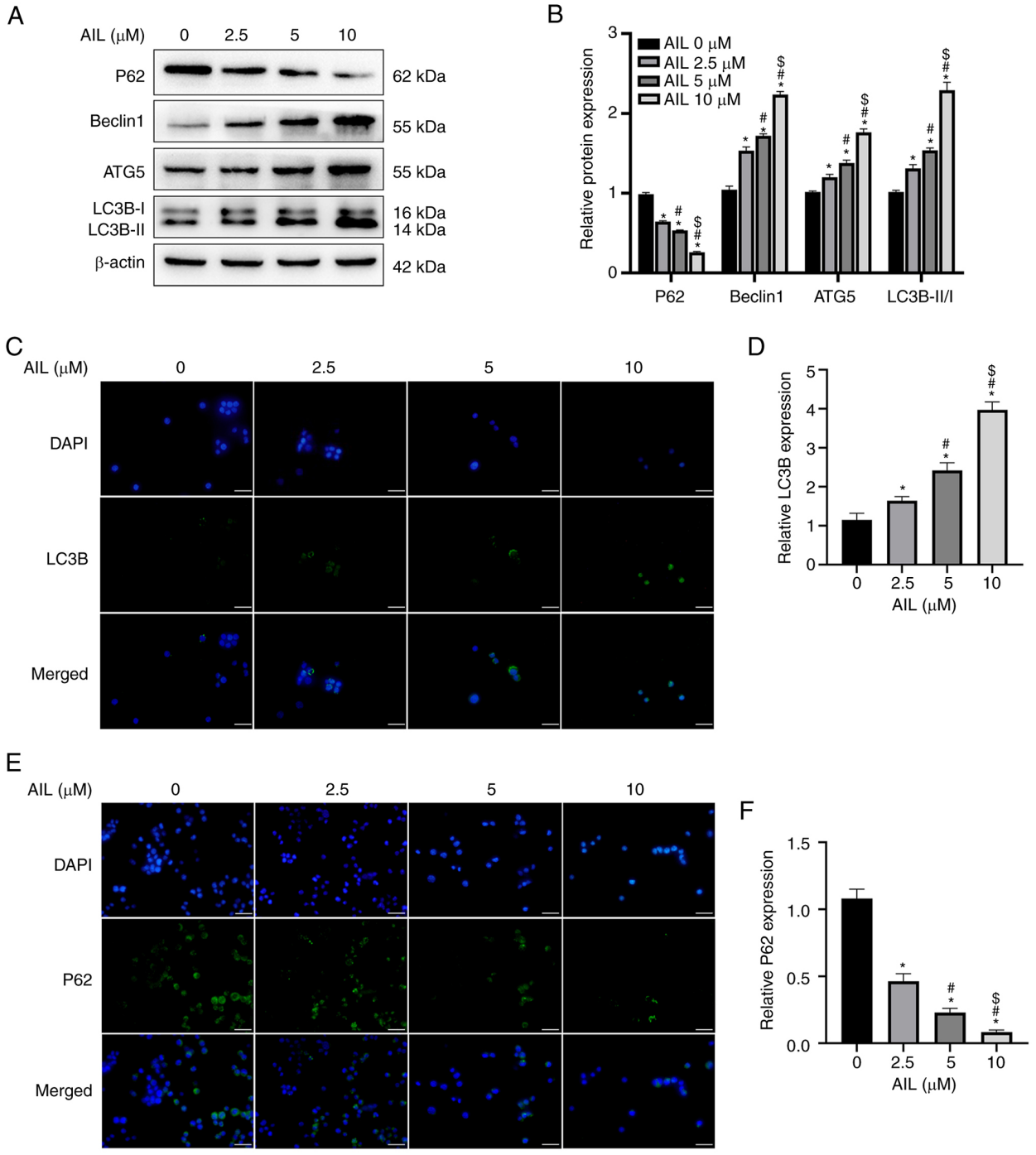

Figure 2. AIL induces autophagy in Lewis cells. (A) Western blot analysis of autophagy-associated proteins P62, Beclin1, ATG5 and LC3 in Lewis cells treated with different concentrations of AIL. (B) Semi-quantitative analysis of the results from the western blot assays. (C) Representative images of LC3B immunostaining in Lewis cells treated with a gradient concentration of AIL. Scale bar, 50 μm. (D) Semi-quantitative analysis of the results from the immunofluorescence assays. (E) Representative images of P62 immunostaining in Lewis cells treated with a gradient concentration of AIL. Scale bar, 50 μm. (F) Semi-quantitative analysis of the results from the immunofluorescence assays. AIL, ailanthone. *P<0.05 vs. AIL 0 μM group; $^{\#}$P<0.05 vs. AIL 2.5 μM group and $^{\$}$P<0.05 vs. AIL 5 μM group.

Iron overload and redox imbalance are the main characteristics of ferroptosis. In this view, the intracellular Fe^{2+} level was detected using an iron assay kit. As demonstrated in Fig. 3D, the intracellular Fe^{2+} content increased (F=353.507; P<0.001) with an increase in AIL concentration. In addition, the effect of AIL on ferroptosis was investigated by assessing the intracellular redox state using reagent kits. The results revealed that the concentrations of LPO (F=380.356; P<0.001; Fig. 3E) and MDA (F=230.938; P<0.001; Fig. 3F) increased, while GSH (F=67.112; P<0.001; Fig. 3G), T-SOD (F=74.961; P<0.001; Fig. 3H) and CAT (F=88.188; P<0.001; Fig. 3I) decreased with an increase in AIL concentration.

In addition, the protein levels of four ferroptosis-associated genes, xCT, GPX4, FTH and TFRC, were evaluated. Western blot assay results revealed that AIL decreased the protein expression levels of xCT (F=2055.887; P<0.001), GPX4 (F=160.192; P<0.001) and FTH (F=402.311; P<0.001) while

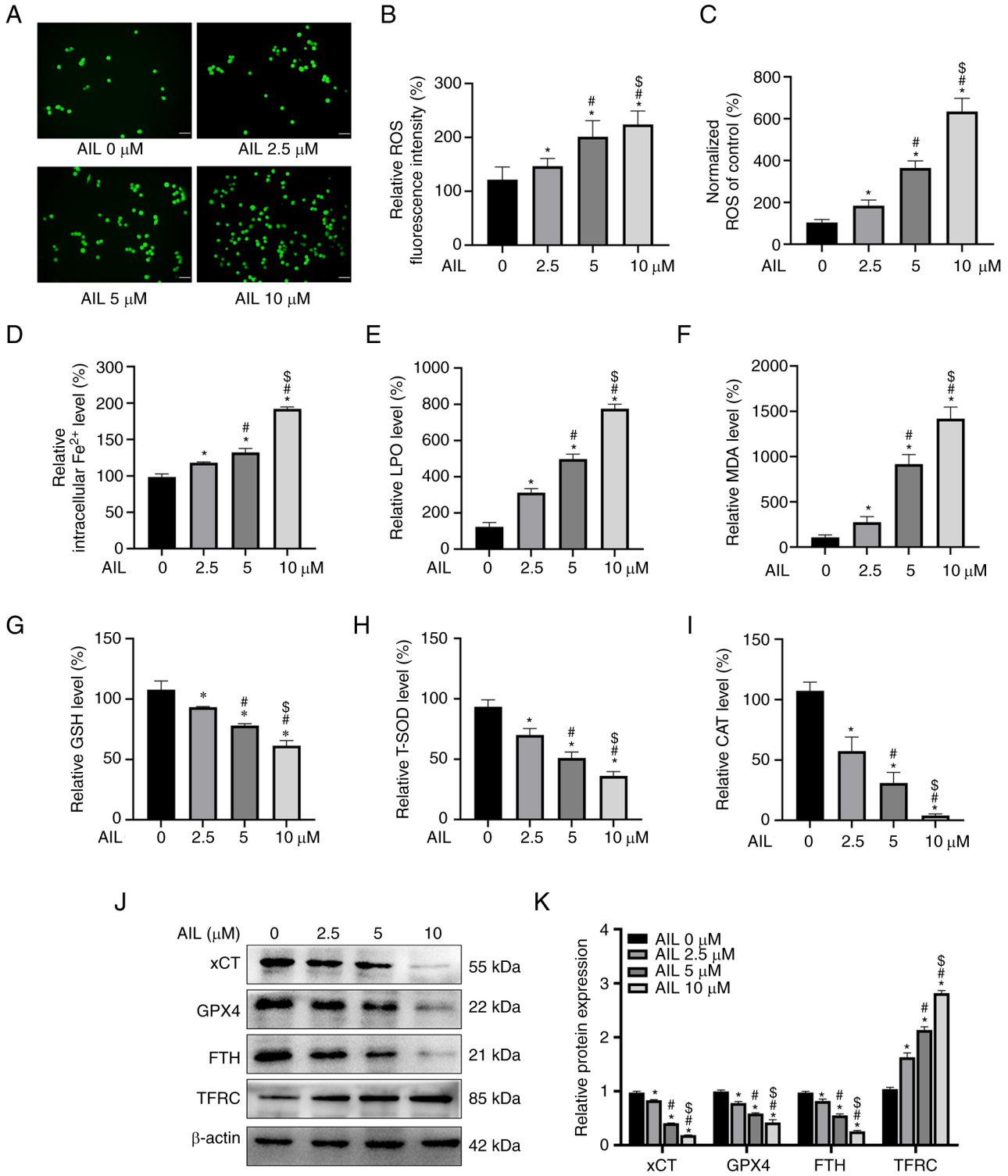

Figure 3. AIL induces ferroptosis in Lewis cells. (A) Relative fluorescence intensity of ROS in Lewis cells treated by AIL under a fluorescence microscope. Scale bar, 50 μm. (B) Semi-quantitative analysis of the results from the fluorescence intensity. (C) Relative fluorescence levels of ROS in Lewis cells treated by AIL, as detected by fluorescent enzyme label. (D-I) Colorimetry detection of the levels of Fe^{2+}, LPO, MDA, GSH, T-SOD and CAT in Lewis cells treated with gradient concentrations of AIL. (J) Western blot analysis of ferroptosis-associated proteins xCT, GPX4, FTH and TFRC in Lewis cells treated with different concentrations of AIL. (K) Semi-quantitative analysis of the results from the western blot assay. *P<0.05 vs. AIL 0 μM group; #P<0.05 vs. AIL 2.5 μM group and $P<0.05 vs. AIL 5 μM group. AIL, ailanthone; ROS, reactive oxygen species; LPO, lipid peroxidation; MDA, malondialdehyde; GSH, glutathione; T-SOD, total superoxide dismutase; CAT, catalase; GPX4, glutathione peroxidase 4; FTH, ferritin heavy chain; TFRC, transferrin receptor.

increasing the protein expression level of TFRC (F=484.205; P<0.001) in Lewis cells in a dose-dependent manner (Fig. 3J and K). These results demonstrated that AIL induces ferroptosis in the NSCLC Lewis cells.

AIL regulates the AMPK/mTOR/p70S6K signaling pathway. The mechanism by which AIL regulates autophagy and ferroptosis was also investigated by evaluating the key protein of the AMPK/mTOR/p70S6K signaling pathway in Lewis cells

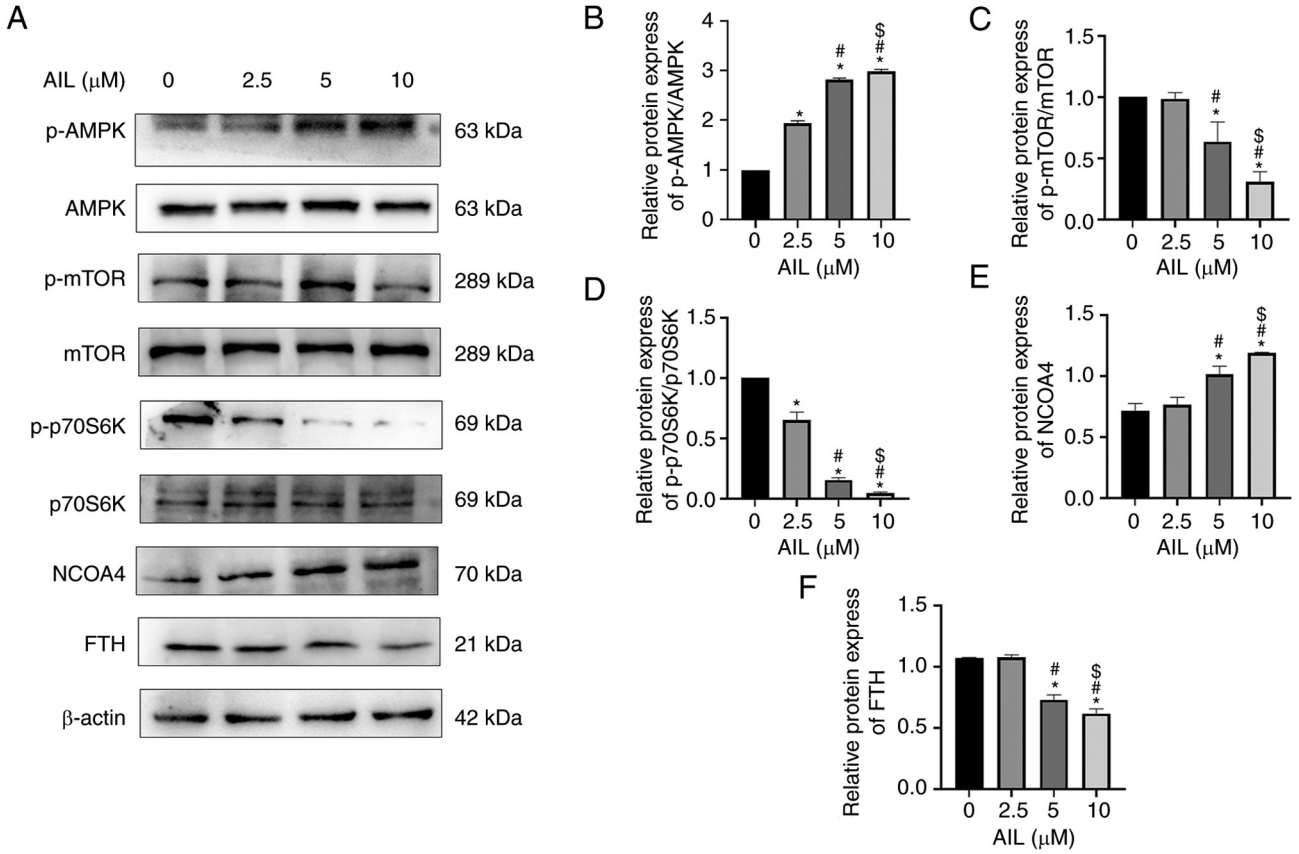

Figure 4. AIL activates the AMPK/mTOR/p70S6K pathway and downstream protein expression in Lewis cells. (A) Western blot detection of the expression levels of key proteins and downstream proteins in the AMPK/mTOR/p70S6K pathway. (B-F) Quantitative results of the relative expression levels of pAMPK/AMPK, pmTOR/mTOR, p-p70S6K/p70S6K, NCOA4 and FTH proteins. *P<0.05 vs. AIL 0 μM group; #P<0.05 vs. AIL 2.5 μM group and $P<0.05 vs. AIL 5 μM group. AIL, ailanthone; p-, phosphorylated; p70S6K, ribosomal protein S6 kinase; NCOA4, nuclear receptor coactivator 4.

treated with a gradient concentration of AIL for 24 h. The results showed that AIL significantly increased p-AMPK levels and p-AMPK/AMPK ratios (F=1199.000; P<0.001; Fig. 4A and B) while decreasing the levels of p-mTOR and p-mTOR/mTOR ratios (F=61.570; P<0.001; Fig. 4A and C), as well as p-p70S6K and p-p70S6K/p70S6K ratios (F=680.200; P<0.001; Fig. 4A and D). Meanwhile, AIL upregulated the pathway downstream protein NCOA4 (F=48.170; P<0.001; Fig. 4A and E), whereas it downregulated FTH protein (F=181.700; P<0.001; Fig. 4A and F).

Discussion

Recent research indicated that an increasing number of Chinese natural medicines have a remarkable antitumor effect while also having fewer side effects (10). In this view, a combination of Chinese natural medicines and antitumor drugs has been used in clinical traditional Chinese medicine antitumor treatment. The present findings demonstrated that AIL significantly suppressed cell proliferation in a dose- and time-dependent way. Indeed, previous research highlighted the anticancer activity of AIL in lung cancer. Ni *et al* (20) found that AIL inhibited cell growth and colony formation in NSCLC cell lines, while also delaying tumor growth and prolonging overall survival in subcutaneous and orthotopic xenograft lung tumor mouse models.

Chen *et al* (21) demonstrated that AIL therapy either significantly up- or downregulated the majority of long non-coding RNAs (lncRNAs) in NSCLC cells. Additionally, AIL-induced alterations in lncRNA expression were essential for the occurrence and metastasis of lung cancer. While these findings revealed that AIL has potent antitumor effects, the underlying mechanism warrants further investigation. As such, current research is focused on regulating autophagy and ferroptosis, the two forms of programmed cell death, in cancer patients (10,20). Wei *et al* (22) identified lower expression of fat atypical cadherin 4 (FAT4) in colorectal cancer tissues than in non-cancerous tissues, and FAT4 could decrease cell proliferation, migration and invasion *in vitro* by promoting autophagy via the PI3K/AKT/GSK-3β and PI3K/AKT/mTOR signaling pathways. Zheng *et al* (23) found that tetrazole blocked lung cancer cell proliferation by over-activating autophagy, which in turn deactivated ERK1/2 signaling while promoting mTOR signaling. Similarly, in the present study it was found that AIL exerted an anti-lung cancer effect by activating autophagy. Expression of autophagy-associated protein in Lewis cells treated with a concentration gradient of AIL was assessed using western blot and immunofluorescence assays. The two detection methods yielded consistent results, with an increase in the expression levels of Beclin1, ATG5 and LC3B and a decrease in P62 protein expression, and these effects were dose-dependent. Various proteins within the cell have been implicated in autophagy regulation. Beclin1 is a crucial autophagy regulator, initiating autophagosome formation by recruiting other autophagy proteins to pre-autophagosomal structures (24). Autophagy activation induces the conversion

of LC3-I into LC3-II, which then associates with autophagic vesicles. Therefore, LC3-II expression and LC3-I transformation to LC3-II are useful indicators for intracellular autophagy assessment (25). Previous evidence indicated that >30 ATGs regulate autophagosome formation, with ATG5 being a central molecule in autophagy elongation (26). Besides, the level of P62 can be utilized as an autophagy indicator because P62 is integrated into mature autophagy and degraded by autophagy. Thus, P62 expression is negatively correlated with autophagy (27). These data suggested that targeting autophagy in cancer may be a promising therapeutic strategy. On one hand, autophagy inducers can prevent the accumulation of damaged proteins and organelles, causing genomic stability and tumor suppression; on the other hand, autophagy inhibitors can restore chemosensitivity and enhance tumor cell death by decreasing stress tolerance and energy production (28).

Previous research has identified ferroptosis as a new form of cell death caused by iron accumulation in the cell and lipid peroxidation (29). Given its vital role in cancer, ferroptosis therapy has become a viable cancer target. Hu *et al* (30) reported that SLC7A11, a critical ferroptosis regulator, was upregulated in lung adenocarcinoma patients with KRAS-mutant and was positively correlated with tumor progression. In another investigation, SLC7A11 inhibitors significantly decreased cystine uptake and glutathione synthesis in cells, which increased oxidative stress- and ER stress-induced cell death in KRAS-mutant cells. ROS plays a crucial role in the ferroptosis mechanism by inducing lipid peroxidation, which consequently results in ferroptosis (31). The present study employed the fluorescent probe DCFH-DA to assess intracellular ROS levels, and the fluorescence intensity was evaluated using a fluorescence microscope and a fluorescence microplate reader. The results revealed higher levels of ROS in Lewis cells treated with different concentrations of AIL. Of note, it was found that ROS accumulation and elevated Fe^{2+} levels induced ferroptosis, and that the level of Fe^{2+} increased with an increase in AIL concentration. Intracellular LPO and MDA are well-known indicators of lipid peroxidation, whereas GSH, T-SOD and CAT are the most commonly used indicators to assess antioxidant potential. In this view, the potential occurrence of ferroptosis in AIL-treated Lewis cells was evaluated. The results demonstrated that an increase in AIL concentration elevated the levels of LPO and MDA while decreasing the levels of GSH, T-SOD and CAT, indicating that AIL increases LPO while decreasing antioxidant enzyme activities, resulting in ferroptosis. In addition, it was identified that AIL treatment decreased the protein expression levels of xCT, GPX4 and FTH but increased the expression of TFRC in Lewis cells. xCT promotes GPX4 activity and lipid oxide metabolism by mediating glutamate export in exchange for cystine (32), ultimately leading to ferroptosis suppression. FTH deficiency and TFRC upregulation result in intracellular iron accumulation, which causes ferroptosis in cancer cells (33). These results demonstrated that AIL increases both lipid peroxidation and ferrous iron accumulation, resulting in ferroptosis.

The AMPK/mTOR/p70S6K signaling pathway is a classical autophagy signaling pathway implicated in ferroptosis. Du *et al* (19) found that dihydroartemisinin increased autophagy by regulating the AMPK/mTOR/p70S6k pathway, eventually causing ferroptosis in acute myeloid leukemia. Chen *et al* (34) demonstrated that amentoflavone inhibited cell proliferation and accelerated cell death by activating autophagy-dependent ferroptosis via the AMPK/mTOR pathway in human glioma. In the present investigation, the expression of the crucial proteins in the AMPK/mTOR/p70S6K signaling pathway was detected after treatment with different AIL concentrations. The results revealed that an increase in AIL concentration increased the pAMPK/AMPK ratio but decreased the ratios of pmTOR/mTOR and p-p70S6K/p70S6K, suggesting that AIL regulates the AMPK/mTOR/p70S6K pathway. Protein phosphorylation denotes signal activation. The upstream adenosine triphosphate and protein kinase drive protein phosphorylation, changing the conformation of receptor protein, which in turn interacts with downstream signaling molecules, initiating a series of cascade reactions downstream of the signal transduction. Generally, the higher the phosphorylation, the stronger the signal activation. In western blot detection, only phosphorylated proteins are considered activated proteins; however, the effect of total protein change cannot be disregarded if only phosphorylated proteins are detected. Hence, the phosphorylated proteins/total protein ratio reflects a more accurate result. A high pAMPK/AMPK ratio is the classical signal of autophagy activation (35). Increased pAMPK/AMPK ratio can decrease pmTOR/mTOR ratio and p-p70S6K/p70S6K ratio, upregulating the expression of autophagy-associated proteins LC3II/I ratio, ATG5 and Beclin-1, and promoting P62 protein degradation (36-39). Meanwhile, it was demonstrated that the ferritinophagy marker NCOA4 was upregulated while the ferroptosis-associated protein, FTH, was downregulated, indicating that AIL also influences the expression of ferroptosis-associated proteins downstream of the AMPK/mTOR/p70S6K pathway.

In conclusion, the present study demonstrated that AIL inhibits proliferation and induces autophagy and ferroptosis in NSCLC Lewis cells by potentially regulating the AMPK/mTOR/p70S6K signaling pathway. However, the link between autophagy and ferroptosis, and whether AIL has an inhibitory effect on NSCLC *in vivo* warrants further investigation.

Acknowledgements

Not applicable.

Funding

The present study was supported by the National Natural Science Foundation of China (grant no. 81703001), the Natural Science Foundation of Hebei (grant no. H2021406021), the Hebei Medical Science Research Project (grant nos. 20210247 and 20221335) and the Hebei Government-Funded Clinical Medical Outstanding Talents Project, Chengde Medical University Scientific Research Major Projects (grant no. KY2020005).

Availability of data and materials

All data generated or analyzed during this study are included in this published article.

Authors' contributions

HY and XZ conceived and designed the experiments. YL and XW visualized data and performed the experiments. ZZ, HX and YB contributed new reagents or analytical tools and designed the methodology. FL, QC and XB analyzed and interpreted the data. LZ and LL contributed to study conception and wrote and reviewed the manuscript. YB and XB confirm the authenticity of all the raw data. All authors read and approved the final version of the manuscript.

Ethics approval and consent to participate

Not applicable.

Patient consent for publication

Not applicable.

Competing interests

The authors declare that they have no competing interests.

References

1. Sung H, Ferlay J and Siegel RL: Global cancer statistics 2020: GLOBOCAN estimates of incidence and mortality worldwide for 36 cancers in 185 countries. CA Cancer J Clin 71: 209-249, 2021.
2. Reck M and Rabe KF: Precision diagnosis and treatment for advanced non-small-cell lung cancer. N Engl J Med 377: 849-861, 2017.
3. Zhang J, Späth SS and Marjani SL: Characterization of cancer genomic heterogeneity by next-generation sequencing advances precision medicine in cancer treatment. Precis Clin Med 1: 29-48, 2018.
4. Yan L, Bao Q, Yang S, Yang M and Mao C: Bionanoparticles in cancer imaging, diagnosis, and treatment. View 20200027, 2022. https://doi.org/10.1002/VIW.20200027.
5. Yin X, Yang J, Zhang M, Wang X, Xu W, Price CH, Huang L, Liu W, Su H, Wang W, *et al*: Serum Metabolic Fingerprints on Bowl-Shaped Submicroreactor Chip for Chemotherapy Monitoring. ACS Nano 16: 2852-2865, 2022.
6. Zhang Y, Zhang C and Min D: Ailanthone up-regulates miR-449a to restrain acute myeloid leukemia cells growth, migration and invasion. ExpMol Pathol 108: 114-120, 2019.
7. He Q, Xiao H and Li J: Fingerprint analysis and pharmacological evaluation of Ailanthus altissima. Int Mol Med 41: 3024-3032, 2018.
8. Zhuo Z, Hu J, Yang X, Chen M, Lei X, Deng L, Yao N, Peng Q, Chen Z, Ye W and Zhang D: Ailanthone inhibits Huh7 cancer cell growth via cell cycle arrest and apoptosis in vitro and in vitro. Sci Rep 5: 16185, 2015.
9. Choi YJ, Park YJ, Park JY, Jeong HO, Kim DH, Ha YM, Kim JM, Song YM, Heo HS, Yu BP, *et al*: Inhibitory effect of mTOR activator MHY1485 on autophagy: suppression of lysosomal fusion. PLoS One 7: e43418, 2012.
10. Klionsky DJ, Abdel-Aziz AK, Abdelfatah S, Abdellatif M, Abdoli A, Abel S, Abeliovich H, Abildgaard MH, Abudu YP, Acevedo-Arozena A, *et al*: Guidelines for the use and interpretation of assays for monitoring autophagy (4th edition). Autophagy 17: 1-382, 2021.
11. Ye J, Zhang R, Wu F, Zhai L, Wang K, Xiao M, Xie T and Sui X: Non-apoptotic cell death in malignant tumor cells and natural compounds. Cancer Lett 420: 210-227, 2018.
12. Liu Y, Yang Y, Ye YC, Shi QF, Chai K, Tashiro S, Onodera S and Ikejima T: Activation of erk-p53 and erk-mediated phosphorylation of Bcl-2 are involved in autophagic cell death induced by the c-met inhibitor su11274 in human lung cancer a549 cells. J Pharmacol Sci 118: 423-432, 2012.
13. Tang D, Kang R, Berghe TV, Vandenabeele P and Kroemer G: The molecular machinery of regulated cell death. Cell Res 29: 347-364, 2019.
14. Guo J, Xu B, Han Q, Zhou H, Xia Y, Gong C, Dai X, Li Z and Wu G: Ferroptosis: A novel anti-tumor action for cisplatin. Cancer Res Treat 50: 445-460, 2018.
15. Bursch W, Ellinger A, Gerner C, Fröhwein U and Schulte-Hermann R: Programmed cell death (PCD), Apoptosis, autophagic PCD, or others? Ann N Y Acad Sci 926: 1-12, 2000.
16. Hou W, Xie Y, Song X, Sun X, Lotze MT, Zeh HJ III, Kang R and Tang D: Autophagy promotes ferroptosis by degradation of ferritin. Autophagy 12: 1425-1428, 2016.
17. Carling D: The AMP-activated protein kinase cascade-a unifying system for energy control. Trends Biochem Sci 29: 18-24, 2004.
18. Kandula N, Kumar S, Mandlem VKK, Siddabathuni A, Singh S and Kosuru R: Role of AMPK in myocardial ischemia-reperfusion injury-induced cell death in the presence and absence of diabetes. Oxid Med Cell Longev 2022: 7346699, 2022.
19. Du J, Wang T, Li Y, Zhou Y, Wang X, Yu X, Ren X, An Y, Wu Y, Sun W, *et al*: DHA inhibits proliferation and induces ferroptosis of leukemia cells through autophagy-dependent degradation of ferritin. Free Radic Biol Med 131: 356-369, 2019.
20. Ni Z, Yao C, Zhu X, Gong C, Xu Z, Wang L, Li S, Zou C and Zhu S: Ailanthone inhibits non-small cell lung cancer cell growth through repressing DNA replication via downregulating RPA1. Br J Cancer 117: 1621-1630, 2017.
21. Chen L, Wu C, Wang H, Chen S, Ma D, Tao Y, Wang X, Luan Y, Wang T, Shi Y, *et al*: Analysis of long noncoding RNAs in aila-induced non-small cell lung cancer inhibition. Front Oncol 11: 652567, 2021.
22. Wei R, Xiao Y, Song Y, Yuan H, Luo J and Xu W: FAT4 regulates the EMT and autophagy in colorectal cancer cells in part via the PI3K-AKT signaling axis. J Exp Clin Cancer Res 38: 112, 2019.
23. Zheng L, Zhang J, Fan J, He Y, Zhan T, Rong L, Yuan M and Zhang H: Lung cancer growth inhibition and autophagy activation by tetrazole via ERK1/2 up-regulation and mTOR/p70S6K signaling down-regulation. Acta Biochim Pol 69: 139-145, 2022.
24. Kang R, Zeh HJ, Lotze MT and Tang D: The Beclin 1 network regulates autophagy and apoptosis. Cell Death Differ 18: 571-580, 2011.
25. Runwal G, Stamatakou E, Siddiqi FH, Puri C, Zhu Y and Rubinsztein DC: LC3-positive structures are prominent in autophagy-deficient cells. Sci Rep 9: 10147, 2019.
26. Mizushima N, Yoshimori T and Ohsumi Y: The role of Atg proteins in autophagosome formation. Annu Rev Cell Dev Biol 27: 107-1 32, 2011.
27. Turco E, Witt M, Abert C, Bock-Bierbaum T, Su MY, Trapannone R, Sztacho M, Danieli A, Shi X, Zaffagnini G, *et al*: FIP200 claw domain binding to p62 promotes autophagosome formation at ubiquitin condensates. Mol Cell 74: 330-346.e11, 2019.
28. Yang ZJ, Chee CE, Huang S and Sinicrope FA: The role of autophagy in cancer: Therapeutic implications. Mol Cancer Ther 10: 1533-1541, 2011.
29. Dixon SJ, Lemberg KM, Lamprecht MR, Skouta R, Zaitsev EM, Gleason CE, Patel DN, Bauer AJ, Cantley AM, Yang WS, *et al*: Ferroptosis: An iron-dependent form of nonapoptotic cell death. Cell 149: 1060-1072, 2012.
30. Hu K, Li K, Lv J, Feng J, Chen J, Wu H, Cheng F, Jiang W, Wang J, Pei H, *et al*: Suppression of the SLC7A11/glutathione axis causes synthetic lethality in Kras-mutant lung adenocarcinoma. Clin Invest 130: 1752-1766, 2020.
31. Su Y, Zhao B, Zhou L, Zhang Z, Shen Y, Lv H, AlQudsy LHH and Shang P: Ferroptosis, a novel pharmacological mechanism of anti-cancer drugs. Cancer Lett 483: 127-136, 2020.
32. Christensen HN: Role of amino acid transport and countertransport in nutrition and metabolism. Physiol Rev 70: 43-77, 1990.
33. Feng H, Schorpp K, Jin J, Yozwiak CE, Hoffstrom BG, Decker AM, Rajbhandari P, Stokes ME, Bender HG, Csuka JM, *et al*: Transferrin receptor is a specific ferroptosis marker. Cell Rep 30: 3411-3423, 2020.
34. Chen Y, Li N, Wang H, Wang N, Peng H, Wang J, Li Y, Liu M, Li H, Zhang Y and Wang Z: Amentoflavone suppresses cell proliferation and induces cell death through triggering autophagy-dependent ferroptosis in human glioma. Life Sci 247: 117425, 2020.
35. Ueno T and Komatsu M: Autophagy in the liver: functions in health and disease. Nat Rev Gastroenterol Hepatol 14: 170-184, 2017.

36. Gu X, Li Y, Chen K, Wang X, Wang Z, Lian H, Lin Y, Rong X, Chu M, Lin J and Guo X: Exosomes derived from umbilical cord mesenchymal stem cells alleviate viral myocarditis through activating AMPK/mTOR-mediated autophagy flux pathway. Cell Mol Med 24: 7515-7530, 2020.
37. Ma S, Yin J, Hao L, Liu X, Shi Q, Diao Y, Yu G, Liu L, Chen J and Zhong J: Exosomes from human umbilical cord mesenchymal stem cells treat corneal injury via autophagy activation. Front Bioeng Biotechnol 10: 879192, 2022.
38. Hou ZP, Li YP, Zhao L, Chen YX and Ruan XZ: Lipopolysaccharide inhibits lipo phagy in HepG2 cells via activating mTOR pathway. Sheng Li Xue Bao 73: 813-820, 2021 (In Chinese).
39. Pinto AP, da Rocha AL, Cabrera EMB, Marafon BB, Kohama EB, Rovina RL, Simabuco FM, Bueno Junior CR, de Moura LP, Pauli JR, *et al*: Role of interleukin-6 in inhibiting hepatic autophagy markers in exercised mice. Cytokine 130: 155085, 2020.